Capillary regression leads to sustained local hypoperfusion by inducing vasoconstriction in upstream transitional vessels

Stephanie K. Bonney[1], Cara D. Nielson[1,2], Maria J. Sosa[1], and Andy Y. Shih[1,3,4]

[1] Center for Developmental Biology and Regenerative Medicine, Seattle Children's Research Institute, Seattle, WA, USA

[2] Graduate Program in Neuroscience, University of Washington, Seattle, WA, USA

[3] Department of Pediatrics, University of Washington, Seattle, WA, USA.

[4] Department of Bioengineering, University of Washington, Seattle, WA, USA.

Correspondence: Andy Y. Shih
Center for Developmental Biology and Regenerative Medicine
Seattle Children's Research Institute
1900 9th Ave. M/S JMB-5
Seattle, WA 98101
Office: 206-884-1314
Fax: 206-884-1407
Email: Andy.Shih@SeattleChildrens.org

ABSTRACT

In the brain, a microvascular sensory web coordinates oxygen delivery to regions with neuronal activity. This involves a dense network of capillaries that send conductive signals upstream to feeding arterioles to promote vasodilation and blood flow. Although this process is critical to the metabolic supply of healthy brain tissue, it may also be a point of vulnerability in disease. Deterioration of capillary networks is a hallmark of many neurological disorders and how this web is engaged during vascular damage remains unknown. We performed *in vivo* two-photon microscopy on young adult mural cell reporter mice and induced focal capillary injuries using precise two-photon laser irradiation on single capillaries. We found that ~63% of the injuries resulted in regression of the capillary segment 7-14 days following injury, and the remaining repaired and re-established blood flow within 7 days of injury. Injuries that resulted in capillary regression induced sustained vasoconstriction in the upstream arteriole-capillary transition (ACT) zone at least 21 days post-injury in both awake and anesthetized mice. This abnormal vasoconstriction involved attenuation of vasomotor dynamics and uncoupling from mural cell-calcium signaling following capillary regression. Consequently, blood flow was reduced in the ACT zone and in secondary, uninjured downstream capillaries. These findings demonstrate how capillary injury and regression, as often seen in age-related neurological disease, can impair the microvascular sensory web and contribute to cerebral hypoperfusion.

SIGNIFICANCE

Deterioration of the capillary network is a hallmark of many neurological diseases and can exacerbate neuronal dysfunction and degeneration due to poor blood perfusion. Here we show that focal capillary injuries can induce vessel regression and elicit sustained vasoconstriction in upstream transitional vessels that branch from cortical penetrating arterioles. This reduces blood flow to broader, uninjured regions of the same microvascular network. These findings suggest that widespread and cumulative damage to brain capillaries in neurological disease may broadly affect blood supply and contribute to disease through their remote actions.

INTRODUCTION

Vascular contributions to cognitive impairment and dementia (VCID) include small, but wide-spread ischemic and hemorrhagic injuries called microinfarctions and microbleeds, respectively[1,2]. These lesions are <3 mm in size and may only occupy 1-2 mL of the total brain volume. However, the remote effects beyond their lesion cores can depress neural function and contribute more broadly to brain dysfunction and cognitive decline[3]. While these micro-lesions are now well recognized features of VCID and believed to result largely from pathologies of brain arterioles, even smaller disruptions are known to occur at the level of capillaries, the finest and most delicate vessels in the brain. Capillaries are the site of amyloid beta buildup during Type 1 cerebral amyloid angiopathy, a form of small vessel disease[4], and reactive oxygen species induced by amyloid beta toxicity can cause damage to the capillary endothelium and neighboring pericytes[5]. Microbleeds can also happen in the absence of capillary amyloid and may result from proteolytic degradation of the endothelium by pericytes or trapped neutrophils[6-8]. These events are a basis for capillary regression and capillary network rarefaction, as commonly seen in aging and VCID[9,10]. Such injuries and events are likely to evade detection by clinical imaging due to their exceedingly small size. While the connection of capillary microbleeds and regression is unknown, together they likely contribute to disease progression in covert and insidious ways. Since the capillary network is dense and redundant in its connectivity[11,12], it is unclear whether focal capillary changes could lead to broader, yet unrecognized detrimental effects on brain perfusion and function.

Capillaries sense neuronal activity via Kir2.1 and TRPA1/Panx1 channels on the endothelium[13,14] and Kir2.2 on pericytes[15]. This initiates a capillary-to-arteriole conductive hyperpolarization that is propagated to upstream arteriole-capillary transitional (ACT) vessels and penetrating arterioles leading to reduced intracellular calcium (Ca^{2+}) and relaxation of smooth muscle cells, and increased blood flow back downstream into the capillary networks [16]. The conductive properties of the microvasculature are dependent upon endothelial and pericyte gap junctions[17]. Vessels within the ACT zone are part of the microvascular inflow tract which are surrounded by ensheathing pericytes and also include precapillary sphincters found just upstream in some vascular brances[18-20]. The ACT zone is highly sensitive to brain activity, as it is the first to dilate during neurovascular coupling.[21,22] But, it is also susceptible to pathology and exhibits sustained constriction after transient cerebral ischemia[23]. Critically, depolarizing electrical stimulation of capillary pericytes leads to a conductive wave of Ca^{2+} increase upstream that elicits robust vasoconstriction in ACT vessels[17]. These findings cast the capillary network as a “sensory

web" that responds to physiological activity and raises the question of how microvascular conductivity behaves in response to pathophysiological events in the capillary network.

To address this open question, we examined how highly focal capillary injuries affect blood flow in their broader microvascular networks. We used *in vivo* two-photon imaging of the mouse cerebral cortex to measure capillary structure and perfusion as well as the dynamics of mural cell Ca^{2+} signaling. Precision laser line-scans were used to induce capillary injury in otherwise healthy vascular networks, and the consequence of this injury was tracked longitudinally over several weeks in anesthetized or awake mice. We asked: (1) How does capillary injury affect the flow and dynamics of upstream ACT and arteriolar zones? (2) Are there lasting effects of capillary injury on blood flow in the respective microvascular networks?

RESULTS

Focal capillary injury induces vessel regression

To understand how capillary injuries may disrupt the microvascular network, we performed *in vivo* two-photon imaging on mural cell reporter mice (PdgfrβCre-tdTomato)[24] and used modified a model of focal capillary injury involving rupture of the vascular wall[25]. Capillaries were identified by distinguishing thin-strand and mesh pericytes on capillary vessels from ensheathing pericytes on ACT vessels[18]. In general, ruptured capillary segments were 5 to 8 branch orders from penetrating arterioles. Injuries were induced by focusing <3 μm diameter circular laser line-scans (~100-154 mW at 800 nm)(**Supp. Fig. 1A**) directly on the vessel lumen as visualized by the perfusion of intravenous (i.v.) dye (70kDa FITC-dextran) (**Fig. 1A**). Laser power was applied in 20 second (s) increments for a total of 20-80 s until there was indication of halting in blood flow and dye leakage (**Fig. 1A, B**). Sham injuries were performed in separate vascular networks using identical laser powers (**Supp. Fig. 1A**) localized next to similarly sized capillary segments (**Supp. Fig. 1B**) without damaging the vessel as indicated by stable vessel diameter following laser irradiation (**Fig. 1B & Supp. Fig. 1C**). Capillary diameter did not influence the laser power or time needed to rupture the vessel (**Supp. Fig. 1D, E**). Although, an increase in laser power, not time, was needed for injuries deeper into the cortex (**Supp. Fig. 1F, G**).

To understand the consequence of focal capillary injury, injured regions were followed for 21 days. One to three days post-injury (dpi) most vessels remained disconnected and lacked blood flow (**Fig. 1B & Supp. Fig. 1H**). Quantification of vessel length demonstrated that the majority of vessels (63% of injuries) had completely receded back to their branch points 7 to 14 dpi (**Fig. 1C**). We defined these as regression events. A smaller portion of injured vessels (37%) reconnected and re-established blood flow 7 dpi (**Fig. 1C & Supp. Fig. 1H**). We defined these as

repair events. Sham injuries did not change the vessel segment length. The occurrence of regression or repair events was not due to differences in laser power, time, diameter or vessel length (**Supp. Fig. 2A-D**). No consistent trend in capillary response was seen with vascular branch order (**Supp. Fig. 2E**), but superficial capillaries (0-50 μm cortical depth) were more likely to regress (**Supp. Fig. 2F**). Overall, these findings show that precision laser line-scans can be used to induce focal capillary injury *in vivo*, with roughly ⅔ of injured vessels experiencing regression and ⅓ undergoing gradual repair.

Pericyte death may be induced by capillary injury, but remodeling of neighboring pericytes ensures coverage.

Following capillary injuries, pericyte death was occasionally observed 3 dpi (22% of injuries), leaving a portion of the capillary network transiently uncovered by pericytes (**Supp. Fig. 3A**). This appeared to be a result of direct or indirect injury, depending on whether the pericyte process was in the laser line-scan path. The somata of dying pericytes were often quite distant from the injury site, highlighting the vulnerability of these cells to injury of a process or perturbations in their microenvironment. In contrast, pericyte loss was not observed following sham injuries, suggesting that local thermal damage to the parenchymal tissue does not drive pericyte loss.

Pericyte death triggered pericyte remodeling, when neighboring pericytes extend their processes into areas of the endothelium lacking pericyte coverage (**Supp. Fig. 3B**)[26,27]. Pericyte process growth was evident at 3 dpi, and in most cases, remodeling was complete by 14 dpi. In sham injuries, pericyte process territory negotiation was occurring based on small local fluctuations in process length, which are known to occur under basal conditions in the healthy mouse brain[26,27] (**Supp. Fig. 3C**). Remodeling pericyte processes achieved an average extension of 62.67 μm, compared to 8.93 μm for negotiating pericytes at sham sites (**Supp. Fig. 3D**). Analysis of uncovered vascular length following pericyte death confirmed that most vessels lacking pericyte contact were recovered by 7-14 dpi (**Supp. Fig. 3E**).

As shown in past studies involving direct ablation of pericytes via their somata[26,27], loss of pericyte coverage with capillary injury resulted in dilation of capillaries (**Supp. Fig. 3F**). On average, uncovered vessels dilated 117.5% from baseline, and returned to their basal diameter following recoverage by pericyte remodeling (**Supp. Fig. 3G**). No significant vessel diameter changes were observed at sham injury sites. Thus, laser-induced capillary injury leads to loss of pericyte coverage in approximately ⅕ of cases, but remodeling of neighboring cells ensures that pericyte coverage is regained over days/weeks.

Focal capillary injury induces a local microglia response

To assess the focality of the capillary injuries, we utilized PdgfrβCre-tdTomato; Cx3cr1-GFP mice to observe microglia activity following injury. We quantified the percent of GFP-positive area within a 25 μm radius surrounding the injury site which appeared to be about the size of the initial microglia response to capillary injury. We found that microglia rapidly migrate to the site 1 dpi (**Fig. 2A, B**). In regression events, microglia occupancy at the injury site remained significantly high 7 and 14 dpi. In contrast, microglial presence at the injury site decreased to baseline 14 dpi in repair events. Sham injuries did not result in a robust or prolonged microglia response at the site of laser ablation (**Fig. 2A, B**). Outside of the irradiation site, we observed no significant change in microglia density surrounding the targeted microvascular network following regression, repair, or sham events (**Fig. 2C**). This demonstrates that laser-induced capillary injury initiates a focal inflammatory response that is prolonged in the event of vessel regression, but does not induce inflammatory conditions along other regions of the vascular network.

Constriction of the arteriole-capillary transition zone following capillary regression

We next aimed to understand the effect of capillary injury on the broader microvascular network. For each experiment, we mapped out the territory of morphologically distinct mural cells along the vascular tree to identify different vascular zones, including the penetrating arteriole, ACT zone, capillaries, and ascending venules (**Fig. 3A**). We then measured the resting diameter of each vessel segment along the mapped microvascular zones to understand if focal capillary injury initiates a response in other vascular zones. Precapillary sphincters were not commonly observed (region of vessel narrowing and distended bulb) in the microvascular networks we examined[19] and were therefore could not be separately assessed in these analyses. We monitored diameter throughout the acute phase, when the injured vessel underwent regression or repair (3-7 dpi), and the chronic phase, when the regression or repair was complete (14-21 dpi). Strikingly, we found a specific decrease in vessel diameter in the upstream ACT zone following capillary regression during both the acute and chronic phases (**Fig. 3B, C**). Some alterations were noted within the capillary zone in the event of regression but did not always maintain a consistent pattern. There were no significant differences in vessel diameter changes across all vascular zones following sham or repair events during acute and chronic phases (**Supp. Fig. 4**). Therefore, repair and sham events were pooled and compared to regression events.

We found ACT zone constriction to be a consistent phenomenon following capillary regression in the acute and chronic phase in experiments when mice underwent imaging in either the anesthetized or awake state (**Fig. 3D**). In the chronic phase, the capillary vessels upstream

from regressed vessels also had decreased diameters during experiments in the anesthetized state. This was not observed in awake imaging experiments. However, prominent constriction of the ACT zone was also evident 10 minutes post capillary injury in awake experiments (**Supp. Fig. 5**). Overall, these data demonstrate that ACT zone constriction is a lasting response detected irrespective of anesthetic state, and is maintained specifically when a capillary regression event occurs as a consequence of distal capillary injury.

Constriction of the arteriole-capillary transition zone is independent of Euclidean and vessel length distance to the site of capillary injury.

We next examined whether likelihood of ACT zone constriction was related to its proximity to the injury site, and thus potential exposure to serum proteins or inflammation. However, the Euclidean and vessel distances between the ACT zone and injury site were comparable between sham/repair and regression events (**Fig. 4A, C**). Furthermore, we did not observe a relationship between the degree of ACT zone constriction with either Euclidean or vessel distance in the acute and chronic phases (**Fig. 4B, D**). This demonstrates that proximity to the injury site was not playing a role in ACT zone constriction.

Vasomotion of the arteriole-capillary transition zone is attenuated and uncoupled from mural cell-Ca^{2+} signaling

Since mural cell-Ca^{2+} signaling regulates vessel diameter in the ACT zone[15,23], we next investigated if resting vasomotion and/or mural cell-Ca^{2+} dynamics were altered in the ACT zone following capillary regression. We performed awake *in vivo* imaging on PdgfrβCre-GCaMP6f mice to observe mural cell-Ca^{2+} and vasomotion during sham and capillary injury experiments. Five minute movies were captured at 2 Hz frequency focusing on the penetrating arteriole and ACT zone (1st and 2nd order vessels) upstream of injuries. By measuring the lumen diameter and GCaMP6f fluorescent intensity of mural cells in the ACT zone (**Fig. 5A**) and penetrating arteriole (**Supp. Fig. 7A**), we were able to study the dynamics and relationship of mural cell-Ca^{2+} and vasomotion during the acute and chronic phases (**Supp. Figs. 6A & 7B**). We performed cross-correlation analysis to identify the timing and strongest coupling between mural cell-Ca^{2+} and vascular diameter, i.e.,“coupling slope”. Diameter changes generally followed fluctuations in mural cell-Ca^{2+} within 1-2 s for both the ACT zone and penetrating arterioles (**Supp. Fig. 6B and 7C**). Following capillary regression, we found a weaker coupling slope in the ACT zone during the acute and chronic phases (**Fig. 5B and Supp. Fig 6B**) but not the penetrating arteriole (**Supp. Fig. 7C, D**). This was a consistent phenomenon following regression events (**Fig. 5C**).

Conversely, sham and repair events maintained strong coupling along ACT vessels and penetrating arterioles throughout the time course.

Interestingly, we found an attenuation of variance in diameter (**Fig. 5D** and **Supp. Fig. 6C**), but not mural cell-Ca^{2+} (**Fig. 5E** and **Supp. Fig. 6D**), in the ACT zone upstream of regressed capillaries. The mean amplitude of vessel diameter oscillations was also reduced (**Supp. Fig. 8A**), although the frequency of vasomotion of ~0.1 Hz was maintained (**Supp. Fig. 8B**). The mean amplitude and frequency of mural cell-Ca^{2+} oscillations were not affected by capillary regression (**Supp Fig. 8C, D**). This highlights a specific disconnect between ACT zone vasodynamics and mural cell-Ca^{2+} following capillary regression. Relatively normal vascular diameter and mural cell-Ca^{2+} variance was maintained along penetrating arterioles following sham, repair and regression events (**Fig. 5D, E, Supp. Fig. 7E, F**). Penetrating arterioles and ACT zones within the imaging field of view, but not directly connected to the injured vessel networks, did not exhibit any alterations to coupling slope or diameter and mural cell-Ca^{2+} variance (**Supp. Fig. 9**). This indicates that constriction of the ACT zone upstream of a regressed vessel results in an attenuation of vasomotion due to uncoupling of mural cell-Ca^{2+} influence on vasomotor activity (**Fig. 5F**).

Constriction of the arteriole-capillary transition zone results in broad blood flow deficits.

To understand the effect of ACT zone constriction on blood flow, we used low power line-scans to track blood cell movement in both the ACT zone and uninjured, secondary capillary off-shoots in awake animals. As predicted, blood volume flux in the ACT zone (**Fig. 6A**) and blood cell flux in the secondary capillary off-shoots (**Fig. 6B**) was reduced for at least 21 days in the event of a capillary regression. This reduction was not observed in sham injuries and repair events. Importantly, lumen diameter was unchanged in the secondary capillary off-shoots, indicating that flow deficits were not due to local capillary constriction (**Fig. 6C**). Rather, the reduction in blood flow in the secondary capillary off-shoots significantly correlated with the reduction in volume flux in the ACT zone (**Fig. 6D**). Thus, ACT zone constriction following capillary regression reduces blood flow into the downstream capillary bed, resulting in broader regions of hypoperfusion (**Fig. 6E**).

DISCUSSION

While the conductive nature of the brain microvasculature is essential for normal blood flow regulation, this trait becomes a potential source of vulnerability in neurological conditions that involve capillary injury. First, we show that injury and regression of single capillaries causes chronic and selective vasoconstriction in the upstream ACT zone, which is located hundreds of

micrometers away but supplies blood to the broader capillary network. Second, this chronic vasoconstriction reduces blood flow to 60-75% of basal levels in the ACT zone and in downstream capillaries, thereby creating an unexpected link between capillary regression and blood flow impairment. Third, capillary regression is associated with reduced amplitude of vasomotor oscillations, where mural cell-Ca^{2+} dynamics are preserved but fail to translate into vascular diameter changes, suggesting a disconnection in actomyosin contraction or relaxation processes.

The ACT zone is where signals converge from the capillary network. Numerous studies have shown that this zone, along with the precapillary sphincter just upstream in some vascular branches, can dilate rapidly to promote blood flow during functional hyperemia[19-21,28]. This zone is also highly sensitive to application of vasoconstrictive mediators such as endothelin-1 and ATP[29]. However, this feature renders the zone more sensitive to tissue pathology. Relating our findings to more complex pathophysiology in models of neurological disease, sustained vasoconstriction in the ACT zone has been reported after reperfusion in both focal and global models of cerebral ischemia[23,30]. In these prior studies, the location of constriction was also most prominent in the ACT zone, compared to upstream penetrating arterioles and downstream capillaries, highlighting the unique reactivity of this zone. Further, vasoconstriction in the ACT zone is observed with potassium-induced cortical spreading depolarization[31], and this may contribute to lasting oligemia following these events. Note that in many prior studies, the ACT zone has also been referred to as “precapillary arterioles” or “first/second order capillaries”, and nomenclature continues to be inconsistent across studies.

The mechanism underlying chronic vasoconstriction in the ACT zone remains unclear. The preservation of Ca^{2+} fluctuations in mural cells suggests that Ca^{2+} handling is intact. Rather, there may be impairment in the expression or function of Ca^{2+}-dependent pathways that stimulate actomyosin cross-bridging (calmodulin and myosin light chain kinase), alpha-smooth muscle actin and myosin, or other cytoskeletal elements that facilitate contractility[32]. Contraction may also be Ca^{2+}-independent. Rho-rho kinase signaling promotes mural cell contraction by inhibiting myosin light chain phosphatase through rho-GTP, and upregulation of this pathway during ischemic injury and subarachnoid hemorrhage is well known[33]. As such, rho kinase inhibitors such as fasudil have utility in attenuating vasospasm to improve blood flow[34]. A further possibility may be excessive vasoconstrictive tone produced by aberrant production of endothelin-1 (ET-1), a potent vasoconstrictor. ET-1 is upregulated in neurological conditions such as hemorrhagic stroke, Alzheimer’s Disease (AD), and multiple sclerosis[35]. It acts through the G-coupled protein receptor, endothelin receptor Type-A, to induce mural cell contraction through Ca^{2+}-dependent and independent mechanisms[36-38]. However, smooth muscle cells and capillary pericytes are also

responsive to ET-1, and why selective ACT zone constriction is observed here remains unclear. Yet another possibility is a physical change in the vessel wall that restrict vasoreactivity, such as thickening in the vascular basement membrane[39]. Further studies are needed to provide deeper mechanistic insight into pathological ACT zone constriction.

We observed a difference in outcome between capillary injuries that involved regression or repair of the targeted capillary even though similar laser irradiation parameters were used (**Suppl. Fig. 2**). The severity of injury was also comparable between groups, as both exhibited initial microbleeds followed by hyper-acute constriction within 10 minutes of injury (**Supp. Fig. 5**). Acute ACT constriction may be an initial response to limit leakage and bleeding following capillary rupture. However, only those involving capillary regression were associated with chronic ACT zone vasoconstriction. It is conceivable that loss of capillary connectivity creates lasting depression or disorganization in endothelial membrane voltage and Ca^{2+} signaling, which reduces input to the ACT zone. While imaging of membrane voltage changes simultaneously across the microvascular network *in vivo* remains technically challenging, recent Ca^{2+} imaging studies have shown complex local Ca^{2+} signals within the endothelium, which are potentiated by conductive hyperpolarizing signals[40]. It is possible that the acute constriction seen in our studies is maintained and repair of the injured capillary segment is needed to regain normal endothelial signaling on a network level and alleviate ACT zone constriction.

Capillary regression is a hallmark of normal aging, AD, VCID, and many other progressive neurological diseases[9,10,41]. In aged animals, the ACT zone and precapillary sphincter exhibit impaired neurovascular coupling responses[42]. This has been attributed to poor responsiveness to vasomodulators, though capillary regression may also be involved. In addition to possible impairment of neurovascular coupling, future studies are needed to identify a co-occurrence of capillary regression with ACT zone constriction in aging and disease. Interestingly, a recent study in the aged mouse brain reported ACT (low order capillary branch) *dilation* associated with age-related capillary density loss. However, cortical depth analysis revealed that deeper cortical layers (Layer 5) exhibit more severe capillary rarefaction and is in fact associated with ACT vasoconstriction[42]. Further, deep two-photon imaging in awake mice showed age-related hypoperfusion was greatest in the callosal white matter[43]. Thus, brain location is key during studies to relate capillary regression with cerebral blood flow.

There are some limitations to these studies. First, it is unclear whether the optical ablation approach produces a form of vascular injury that is representative of disease pathology. Therefore, other targeted approaches to induce capillary regression in a zone-specific manner will be instructive to test whether this phenomenon is technique specific. Second, although our

targeted, minimalistic approach was necessary to reveal pathophysiological communication between vascular zones, we did not examine correlation between capillary regression and ACT constriction in mouse models of disease. Due to the complex nature of vascular pathology in disease models, only correlative results would be garnered from these efforts. However, future studies could examine whether comorbid factors such as age, hypertension, or cerebral small vessel disease modify the effects we have observed in healthy adult mice. Third, our studies are restricted to relatively superficial layers of cortex (upper 200 μm) because optical ablations could only be effectively generated at these depths due to light scattering. Layer specific differences in vascular vulnerability and architecture will need to be considered in future studies.

In summary, our studies reveal a new dimension into how capillary-level pathology can produce outsized effects on perfusion by acting upon upstream ACT vessels. This link may be a contributing factor in the cerebral hypoperfusion detected in VCID, AD, and chronic phases of acute neurological injuries (stroke, hemorrhage, traumatic brain injury). The ACT zone is a crucial control point for delivery of blood into the capillary network. Thus, it is imperative to understand how ACT dysfunction arises in disease, since therapeutic modulation of this vascular zone may improve and maintain cerebral blood flow.

MATERIALS & METHODS

Animals. Mice were housed in a specific pathogen-free facility approved by AALAC and were handled in accordance with protocols approved by the Seattle Children's Research Institute IACUC committee. PdgfrβCre-tdTomato and PdgfrβCre-GCaMP6f mice were created by breeding Pdgfrβ-Cre mice (FVB and C57BL/6 × 129 background)[44] with Ai14-flox (Jax #007914)[45] or Ai95-flox (Jax #028865)[46] mice (C57BL/6 backgrounds) to generate mural cell reporter lines. PdgfrβCre-tdTomato mice were crossed with Cx3cr1-GFP (Jax #005582) mice (C57BL/6 background)[47] to simultaneously label mural cells and microglia. Pdgfrβ-Cre mice were a generous gift from Prof. Volkhard Lindner of the Maine Medical Center Research Institute. Both male and female mice within 3-8 months of age were utilized.

Cranial window surgery and in vivo two-photon imaging. Chronic, skull-removed cranial windows were placed over the somatosensory cortex for *in vivo* imaging, as previously described[26]. Mice were allowed to recover for at least three weeks prior to imaging. For vascular labeling, various fluorescent dextrans were injected retro-orbitally under deep isoflurane anesthesia (2% MAC in medical-grade air). PdgfrβCre-tdTomato mice were injected with 25 μL of 5% (w/v in saline) 70kDa FITC-dextran (Sigma-Aldrich; 46945), PdgfrβCre-tdTomato; Cx3cr1-GFP mice were

injected with 25 μL of 5% (w/v in saline) custom Alexa Fluor 680 (Life Technologies; A20008) conjugated to 2MDa Dextran (Fisher Scientific; NC1275021)[48], and PdgfrβCre-Ai95 mice were injected with 25 μL of 2.5% (w/v in saline) 70kDa Texas Red™ dextran (Invitrogen™; D1864). During imaging of PdgfrβCre-tdTomato and PdgfrβCre-tdTomato; Cx3cr1-GFP mice, isoflurane was maintained at ~1.5% MAC in medical-grade air. PdgfrβCre-Ai95 mice were habituated for awake imaging during a 1-2 hour imaging session while head fixed to a free-moving treadmill prior to experiments. During imaging experiments, mice were allowed to wake up for 10 minutes following administration of the i.v. dye while under brief isoflurane anesthesia. Imaging was performed with a Bruker Investigator coupled to a Spectra-Physics Insight X3. The laser was tuned for 975 nm excitation when imaging PdgfrβCre-tdTomato mice, and 920 nm excitation was used for PdgfrβCre-tdTomato; Cx3cr1-GFP and PdgfrβCre-Ai95 mice. Collection of green, red and far-red fluorescence emission was achieved with 525/70, 595/50, and 660/40 emission bandpass filters respectively, and detected with Hamamatsu GaAsP photomultiplier tubes. A 20x (1.0 NA) water-immersion objective (Olympus; XLUMPLFLN) was used to collect high-resolution images. For structural imaging of the brain vasculature, z-stacks were collected at 1.0 μm z increments at 347 μm x 347 μm (512 x 512 pixel resolution) using 3.6 μs/pixel dwell time. For imaging of mural cell Ca^{2+} signaling and vasomotion in PdgfrβCre-Ai95 mice, movies were captured for 307.2 s at 1.951 Hz at 295 μm x 295 μm (256 x 256 pixel resolution) using 1.2 μs/pixel dwell time. For blood flow analysis, three trials of line-scans for 1.3 s were drawn along the ACT zone (1st and 2nd order vessels) and uninjured, secondary capillaries.

Capillary injury using two-photon irradiation. Capillary segments to target for injuries were chosen by identifying capillary segments both within the upper 200 μm of cortex and greater than 4 branch orders from a penetrating arteriole. Injuries were induced by creating a circular line-scan path (<3 μm in diameter) to target ~100-154 mW of power at 800 nm excitation directly onto the vessel lumen for 20-80 s in 20 s increments at 3.6 μs/pixel dwell time. Scanning was stopped when blood flow halted (stalled dye and/or red blood cells) and leakage of i.v. dye was observed. Sham injuries were performed in separate vascular networks using similar parameters focused on a parenchymal region adjacent to a capillary segment.

Analysis of pericyte remodeling, vessel coverage, and pericyte-associated diameter changes. To analyze pericyte remodeling following capillary injury-induced pericyte death, remodeling processes were first identified by determining which processes of neighboring pericytes had lost pericyte contact at their terminal tips. Then, using the simple neurite tracer (SNT) plugin in FIJI, process length was measured from soma to process terminus at each imaging time point[26].

Process extension was calculated by subtracting process length at baseline from process length at each imaging time point. Vascular length uncovered by pericytes at each time point was also measured using SNT in FIJI and percent vessel coverage was based on uncovered vessel length 1 dpi. Vessel diameter was determined in pre-injury images (prior to pericyte death), the uncovered state (3 dpi) and the recovered state (14 dpi) using the VasoMetrics FIJI plugin[49].

Quantification of the microglia response to focal capillary injury. The percent of GFP-positive area in the 25 μm radius surrounding the injury site and the number of microglia surrounding targeted microvascular zones was measured in FIJI at each time point. All images for Cx3cr1-GFP area analysis were thresholded prior to analysis.

Topological analysis of vessel diameter. To analyze vessel diameter changes across the microvascular web following capillary injury and sham experiments, the territory of capillary pericytes along the vascular tree was mapped out using the SNT FIJI plugin to identify how each microvascular zone connects from penetrating arteriole to ascending venule. Experiments in which pericytes died due to capillary injury were not included. Vessel diameter at each branch point was measured in FIJI using the VasoMetrics plugin on max projections of each vessel segment[49]. Vessel segments were measured at each timepoint and the percent change was calculated based on pre-injury vessel diameter.

Analysis of distance between the injury site and the ACT zone. To measure the Euclidean distance between the injury site and the ACT zone, the distance between the focal plane of the injury site and the focal plane of the ACT zone (z) was determined. Then, the distance between the injury site and the ACT zone (d) was measured using the line function in FIJI on the max projected image. The equation $\sqrt{z^2 + d^2}$ was used to calculate the Euclidean distance. To measure the vessel distance between the injury site and the ACT zone, the length of each vessel segment between the two sites was measured using the SNT FIJI plugin.

Analysis of vasomotion and mural cell-Ca^{2+} dynamics. In awake PdgfrβCre-Ai95 mice, movies were collected of smooth muscle cells on penetrating arterioles and ensheathing pericytes on the 1st and 2nd order ACT zone upstream of each injury. Frames containing movement and ~10 s after were excluded to only analyze resting vasomotion. To analyze vasomotion, the VasoMetrics plugin was utilized to measure vessel diameter in each frame[49]. To analyze mural cell-Ca^{2+} signatures in FIJI, images were despeckled and a ROI was drawn around the smooth muscle cells and ensheathing pericyte processes. The fluorescent intensity profile throughout the time series data was obtained using the plot z-axis profile function and the change in fluorescence

divided by the median fluorescence intensity (dF/F0) was calculated. Vessel diameter and dF/F0 were plotted against each other to analyze their relationship. The coupling slope was determined by performing a cross-correlation analysis at each time point to determine the strongest inverse relationship. Raw data was used to calculate the linear regression, cross-correlation, amplitude, frequency and variance. For frequency and power analysis, MATLAB was used to bandpass filter signals from 0.025 – 0.2 Hz, the frequency range known to represent vasomotor activity[50], and the average frequency and power were calculated. Data shown in Supplemental Figures 6A and 7B are smoothed data with a running average window of 5 data points to better show the trend of Ca^{2+} signatures and vasomotion.

Blood flow analysis. Following collection of blood flow images using line-scan function, red blood cell (RBC) velocity was measured in the ACT zone using MATLAB code for line-scanning particle image velocimetry[51] and blood volume flux was calculated using $F=\frac{1}{8}(\pi)(\text{velocity})(\text{diameter})^2$. In the secondary capillary offshoots, RBC flux was measured by counting the number of RBC shadows in each line-scan using the CellCounter plugin in FIJI and normalizing the numbers to represent flux over a 1 s period. Blood flow measurements from the 3 line-scans were averaged to achieve the final result.

*Statistics***.** All statistical analyses were performed in Graphpad Prism (ver. 9). Respective statistical analyses are reported in each figure legend. Normality tests, generally Shapiro-Wilk tests, were performed on necessary data sets prior to statistical tests. Standard deviation is reported in all graphs where necessary.

FUNDING

SKB was supported by fellowships from the NIH/NINDS (F32NS117649) and NIH/NIA (K99AG080034). CDN was supported by a NIH training grant (T32AG052354). MJS was supported by a Diversity supplement for a grant from the NIH/NIA (R01AG062738). AYS and projects in the Shih lab were supported by grants from the NIH/NIA (R01AG062738, R21AG069375, RF1AG077731, R01AG081840).

AUTHOR CONTRIBUTIONS

SKB, CDN, and AYS conceptualized and designed experiments. Two-photon imaging and data analysis was done by SKB, CDN, and MJS. Statistics was performed by SKB and CDN. Manuscript was written by SKB, CDN and AYS with editing and contributions from all authors.

CONFLICT OF INTEREST

The authors have no financial or non-financial conflicts of interest.

REFERENCES

1. van Veluw SJ, Shih AY, Smith EE, et al. Detection, risk factors, and functional consequences of cerebral microinfarcts. *Lancet Neurol*. Sep 2017;16(9):730-740. doi:10.1016/S1474-4422(17)30196-5
2. Greenberg SM, Vernooij MW, Cordonnier C, et al. Cerebral microbleeds: a guide to detection and interpretation. *Lancet Neurol*. Feb 2009;8(2):165-74. doi:10.1016/S1474-4422(09)70013-4
3. Summers PM, Hartmann DA, Hui ES, et al. Functional deficits induced by cortical microinfarcts. *J Cereb Blood Flow Metab*. Nov 2017;37(11):3599-3614. doi:10.1177/0271678X16685573
4. Thal DR, Ghebremedhin E, Rüb U, Yamaguchi H, Del Tredici K, Braak H. Two types of sporadic cerebral amyloid angiopathy. *J Neuropathol Exp Neurol*. Mar 2002;61(3):282-93. doi:10.1093/jnen/61.3.282
5. Nortley R, Korte N, Izquierdo P, et al. Amyloid β oligomers constrict human capillaries in Alzheimer's disease via signaling to pericytes. *Science*. 07 19 2019;365(6450)doi:10.1126/science.aav9518
6. Turner RJ, Sharp FR. Implications of MMP9 for Blood Brain Barrier Disruption and Hemorrhagic Transformation Following Ischemic Stroke. *Front Cell Neurosci*. 2016;10:56. doi:10.3389/fncel.2016.00056
7. Underly RG, Levy M, Hartmann DA, Grant RI, Watson AN, Shih AY. Pericytes as Inducers of Rapid, Matrix Metalloproteinase-9-Dependent Capillary Damage during Ischemia. *J Neurosci*. 01 2017;37(1):129-140. doi:10.1523/JNEUROSCI.2891-16.2016
8. Fisher M, French S, Ji P, Kim RC. Cerebral microbleeds in the elderly: a pathological analysis. *Stroke*. Dec 2010;41(12):2782-5. doi:10.1161/STROKEAHA.110.593657
9. Schager B, Brown CE. Susceptibility to capillary plugging can predict brain region specific vessel loss with aging. *J Cereb Blood Flow Metab*. 12 2020;40(12):2475-2490. doi:10.1177/0271678X19895245
10. van Dinther M, Voorter PH, Jansen JF, et al. Assessment of microvascular rarefaction in human brain disorders using physiological magnetic resonance imaging. *J Cereb Blood Flow Metab*. May 2022;42(5):718-737. doi:10.1177/0271678X221076557
11. Blinder P, Tsai PS, Kaufhold JP, Knutsen PM, Suhl H, Kleinfeld D. The cortical angiome: an interconnected vascular network with noncolumnar patterns of blood flow. *Nat Neurosci*. Jul 2013;16(7):889-97. doi:10.1038/nn.3426
12. Nishimura N, Schaffer CB, Friedman B, Tsai PS, Lyden PD, Kleinfeld D. Targeted insult to subsurface cortical blood vessels using ultrashort laser pulses: three models of stroke. *Nat Methods*. Feb 2006;3(2):99-108. doi:10.1038/nmeth844
13. Longden TA, Dabertrand F, Koide M, et al. Capillary K. *Nat Neurosci*. May 2017;20(5):717-726. doi:10.1038/nn.4533
14. Thakore P, Alvarado MG, Ali S, et al. Brain endothelial cell TRPA1 channels initiate neurovascular coupling. *Elife*. Feb 26 2021;10doi:10.7554/eLife.63040
15. Glück C, Ferrari KD, Binini N, et al. Distinct signatures of calcium activity in brain mural cells. *Elife*. 07 06 2021;10doi:10.7554/eLife.70591
16. Hartmann DA, Coelho-Santos V, Shih AY. Pericyte Control of Blood Flow Across Microvascular Zones in the Central Nervous System. *Annu Rev Physiol*. Feb 10 2022;84:331-354. doi:10.1146/annurev-physiol-061121-040127
17. Kovacs-Oller T, Ivanova E, Bianchimano P, Sagdullaev BT. The pericyte connectome: spatial precision of neurovascular coupling is driven by selective connectivity maps of

pericytes and endothelial cells and is disrupted in diabetes. *Cell Discov*. 2020;6:39. doi:10.1038/s41421-020-0180-0

18. Grant RI, Hartmann DA, Underly RG, Berthiaume AA, Bhat NR, Shih AY. Organizational hierarchy and structural diversity of microvascular pericytes in adult mouse cortex. *J Cereb Blood Flow Metab*. 03 2019;39(3):411-425. doi:10.1177/0271678X17732229
19. Grubb S, Cai C, Hald BO, et al. Precapillary sphincters maintain perfusion in the cerebral cortex. *Nat Commun*. 01 20 2020;11(1):395. doi:10.1038/s41467-020-14330-z
20. Zambach SA, Cai C, Helms HCC, et al. Precapillary sphincters and pericytes at first-order capillaries as key regulators for brain capillary perfusion. *Proc Natl Acad Sci U S A*. Jun 29 2021;118(26)doi:10.1073/pnas.2023749118
21. Hall CN, Reynell C, Gesslein B, et al. Capillary pericytes regulate cerebral blood flow in health and disease. *Nature*. Apr 2014;508(7494):55-60. doi:10.1038/nature13165
22. Rungta RL, Chaigneau E, Osmanski BF, Charpak S. Vascular Compartmentalization of Functional Hyperemia from the Synapse to the Pia. *Neuron*. Jul 25 2018;99(2):362-375.e4. doi:10.1016/j.neuron.2018.06.012
23. Hill RA, Tong L, Yuan P, Murikinati S, Gupta S, Grutzendler J. Regional Blood Flow in the Normal and Ischemic Brain Is Controlled by Arteriolar Smooth Muscle Cell Contractility and Not by Capillary Pericytes. *Neuron*. Jul 2015;87(1):95-110. doi:10.1016/j.neuron.2015.06.001
24. Hartmann DA, Underly RG, Grant RI, Watson AN, Lindner V, Shih AY. Pericyte structure and distribution in the cerebral cortex revealed by high-resolution imaging of transgenic mice. *Neurophotonics*. Oct 2015;2(4):041402. doi:10.1117/1.NPh.2.4.041402
25. Taylor S, Mehina E, White E, et al. Suppressing Interferon-γ Stimulates Microglial Responses and Repair of Microbleeds in the Diabetic Brain. *J Neurosci*. Oct 03 2018;38(40):8707-8722. doi:10.1523/JNEUROSCI.0734-18.2018
26. Berthiaume AA, Grant RI, McDowell KP, et al. Dynamic Remodeling of Pericytes In Vivo Maintains Capillary Coverage in the Adult Mouse Brain. *Cell Rep*. 01 2018;22(1):8-16. doi:10.1016/j.celrep.2017.12.016
27. Berthiaume AA, Schmid F, Stamenkovic S, et al. Pericyte remodeling is deficient in the aged brain and contributes to impaired capillary flow and structure. *Nat Commun*. Oct 07 2022;13(1):5912. doi:10.1038/s41467-022-33464-w
28. Rungta RL, Chaigneau E, Osmanski BF, Charpak S. Vascular Compartmentalization of Functional Hyperemia from the Synapse to the Pia. *Neuron*. Feb 20 2019;101(4):762. doi:10.1016/j.neuron.2019.01.060
29. Cai C, Fordsmann JC, Jensen SH, et al. Stimulation-induced increases in cerebral blood flow and local capillary vasoconstriction depend on conducted vascular responses. *Proc Natl Acad Sci U S A*. Jun 19 2018;115(25):E5796-E5804. doi:10.1073/pnas.1707702115
30. Hauck EF, Apostel S, Hoffmann JF, Heimann A, Kempski O. Capillary flow and diameter changes during reperfusion after global cerebral ischemia studied by intravital video microscopy. *J Cereb Blood Flow Metab*. Apr 2004;24(4):383-91. doi:10.1097/00004647-200404000-00003
31. Khennouf L, Gesslein B, Brazhe A, et al. Active role of capillary pericytes during stimulation-induced activity and spreading depolarization. *Brain*. Jul 01 2018;141(7):2032-2046. doi:10.1093/brain/awy143
32. Erdener Ş, Küreli G, Dalkara T. Contractile apparatus in CNS capillary pericytes. *Neurophotonics*. Apr 2022;9(2):021904. doi:10.1117/1.NPh.9.2.021904
33. Shin HK, Salomone S, Ayata C. Targeting cerebrovascular Rho-kinase in stroke. *Expert Opin Ther Targets*. Dec 2008;12(12):1547-64. doi:10.1517/14728220802539244
34. Zhao J, Zhou D, Guo J, et al. Effect of fasudil hydrochloride, a protein kinase inhibitor, on cerebral vasospasm and delayed cerebral ischemic symptoms after aneurysmal

subarachnoid hemorrhage. *Neurol Med Chir (Tokyo)*. Sep 2006;46(9):421-8. doi:10.2176/nmc.46.421
35. Barton M, Yanagisawa M. Endothelin: 30 Years From Discovery to Therapy. *Hypertension*. Dec 2019;74(6):1232-1265. doi:10.1161/HYPERTENSIONAHA.119.12105
36. Kowalczyk A, Kleniewska P, Kolodziejczyk M, Skibska B, Goraca A. The role of endothelin-1 and endothelin receptor antagonists in inflammatory response and sepsis. *Arch Immunol Ther Exp (Warsz)*. Feb 2015;63(1):41-52. doi:10.1007/s00005-014-0310-1
37. Miyoshi Y, Nakaya Y, Wakatsuki T, et al. Endothelin blocks ATP-sensitive K+ channels and depolarizes smooth muscle cells of porcine coronary artery. *Circ Res*. Mar 1992;70(3):612-6. doi:10.1161/01.res.70.3.612
38. Park WS, Ko EA, Han J, Kim N, Earm YE. Endothelin-1 acts via protein kinase C to block KATP channels in rabbit coronary and pulmonary arterial smooth muscle cells. *J Cardiovasc Pharmacol*. Feb 2005;45(2):99-108. doi:10.1097/01.fjc.0000150442.49051.f7
39. Thomsen MS, Routhe LJ, Moos T. The vascular basement membrane in the healthy and pathological brain. *J Cereb Blood Flow Metab*. Oct 2017;37(10):3300-3317. doi:10.1177/0271678X17722436
40. Longden TA, Mughal A, Hennig GW, et al. Local IP. *Sci Adv*. Jul 2021;7(30)doi:10.1126/sciadv.abh0101
41. Steinman J, Sun HS, Feng ZP. Microvascular Alterations in Alzheimer's Disease. *Front Cell Neurosci*. 2020;14:618986. doi:10.3389/fncel.2020.618986
42. Cai C, Zambach SA, Grubb S, et al. Impaired dynamics of precapillary sphincters and pericytes at first-order capillaries predict reduced neurovascular function in the aging mouse brain. *Nat Aging*. Feb 2023;3(2):173-184. doi:10.1038/s43587-022-00354-1
43. Shin P, Pian Q, Ishikawa H, et al. Aerobic exercise reverses aging-induced depth-dependent decline in cerebral microcirculation. *bioRxiv*. Feb 13 2023;doi:10.1101/2023.02.12.528244
44. Cuttler AS, LeClair RJ, Stohn JP, et al. Characterization of Pdgfrb-Cre transgenic mice reveals reduction of ROSA26 reporter activity in remodeling arteries. *Genesis*. Aug 2011;49(8):673-80. doi:10.1002/dvg.20769
45. Madisen L, Zwingman TA, Sunkin SM, et al. A robust and high-throughput Cre reporting and characterization system for the whole mouse brain. *Nat Neurosci*. Jan 2010;13(1):133-40. doi:10.1038/nn.2467
46. Tian L, Hires SA, Mao T, et al. Imaging neural activity in worms, flies and mice with improved GCaMP calcium indicators. *Nat Methods*. Dec 2009;6(12):875-81. doi:10.1038/nmeth.1398
47. Jung S, Aliberti J, Graemmel P, et al. Analysis of fractalkine receptor CX(3)CR1 function by targeted deletion and green fluorescent protein reporter gene insertion. *Mol Cell Biol*. Jun 2000;20(11):4106-14. doi:10.1128/MCB.20.11.4106-4114.2000
48. Li B, Ohtomo R, Thunemann M, et al. Two-photon microscopic imaging of capillary red blood cell flux in mouse brain reveals vulnerability of cerebral white matter to hypoperfusion. *J Cereb Blood Flow Metab*. 03 2020;40(3):501-512. doi:10.1177/0271678X19831016
49. McDowell KP, Berthiaume AA, Tieu T, Hartmann DA, Shih AY. VasoMetrics: unbiased spatiotemporal analysis of microvascular diameter in multi-photon imaging applications. *Quant Imaging Med Surg*. Mar 2021;11(3):969-982. doi:10.21037/qims-20-920
50. van Veluw SJ, Hou SS, Calvo-Rodriguez M, et al. Vasomotion as a Driving Force for Paravascular Clearance in the Awake Mouse Brain. *Neuron*. 02 2020;105(3):549-561.e5. doi:10.1016/j.neuron.2019.10.033
51. Kim TN, Goodwill PW, Chen Y, et al. Line-scanning particle image velocimetry: an optical approach for quantifying a wide range of blood flow speeds in live animals. *PLoS One*. 2012;7(6):e38590. doi:10.1371/journal.pone.0038590

FIGURE LEGENDS

Figure 1 – Focal capillary injury induced by optical laser ablation.

(A) Graphical depiction of a cortical microvascular network with location of two-photon laser-induced capillary injury. Microvascular zones are highlighted including the pial artery and penetrating arteriole (red), arteriole-capillary transition zone (orange), capillary zone (green), ascending venule and pial vein (blue). **(A')** Representative *in vivo* image of a capillary injury in a PdgfrβCre-tdTomato mouse pre-injury with line-scan path (cyan) and ~10 minutes post-injury. Pericytes are shown in red and i.v. dye (70kDa FITC-Dextran) labeling vessels in green.

(B) Representative *in vivo* images of a capillary regression, repair, and sham event pre- and post-injury (~10 minutes), and then at various days post-laser-induced injury.

(C) Graphs of percent change in length of the injured (gray; left) or sham (black; right) capillaries based on visible i.v. dye in the lumen pre-injury (0 day) and various days post-injury. Overall, 10/27 injuries (37%) resulted in capillary repairs and 17/27 (63%) resulting in regressions, in experiments conducted over 14 mice. Sham injuries = 15 conducted over 12 mice.

Figure 2 – Microglia activation is concentrated only around injury site

(A) Representative *in vivo* image of a capillary injury in a PdgfrβCre-tdTomato; Cx3cr1-GFP mouse pre, post (~10 minutes), 1-, and 14-days post-capillary injury. Pericytes are shown in red, microglia in green, and i.v. dye (2MDa Alexa 680-Dextran) labeling vessels depicted in blue. Microvascular zones such as penetrating arteriole (PA), arteriole-capillary transition (ACT) zone, and ascending venules (AVs) are shown to depict the highly focal nature of the laser-induced capillary injuries and resulting neuroinflammatory reaction (25 μm radius; white dashed circle).

(B) Graph of percent area of Cx3cr1-GFP+ microglia at injury site pre-injury (0 day) and 1-, 7-, and 14-days post-injury. Dunnett's multiple comparison test: Regression event: 0 vs. 1 day **p=0.0074, 0 vs. 7 days: *p=0.0109, 0 vs 14 days: *p=0.0385. Sham injuries n=3, regression events n=3, repair events n=3; 2 mice.

(C) Graph of Cx3cr1-GFP+ microglia density surrounding injury site (~$6m^3$ analyzed region, excluding injury site) pre-injury (0 day) and 1-, 7-, and 14-days post-injury. Dunnett's multiple comparison test was performed and no significant differences were detected in microglia density.

Figure 3 – Chronic constriction of arteriole-capillary transition vessels occurs following laser-induced capillary regression.

(A) Graphical depiction of vessel network mapping by tracing pericyte territories (pink) and branch order from penetrating arteriole (PA) and arteriole-capillary transition (ACT) zone through the capillary network including the injury site to the ascending venule (AV). **(A')** Representative *in vivo* image of a capillary injury with pericyte territories in a PdgfrβCre-tdTomato mouse pre-injury with the line-scan path (cyan) and ~10 minutes post-injury (inset). Pericyte territories in pink with branch order and blood flow direction (dash line and arrow) denoted. Pericytes are shown in red and i.v. dye (70kDa FITC-Dextran) labeling vessels depicted in green and grayscale.
(B) Graph of percent change in vessel diameter from baseline across the microvascular zones (PA, ACT, Capillary, AV) in a vessel network of a sham (black), regression (purple), and repair (blue) event. Changes in diameter are reported for each branch order in the acute phase (3 and 7 days) and the chronic phase (14 and 21 days). Branch order of injury sites in the capillary networks of the three case examples are denoted with color coded arrows.
(C) Representative *in vivo* image of upstream ACT vessel segments from a sham, regression, and repair event pre-injury and in the acute and chronic phase following capillary injury. Pericytes are shown in red and i.v. dye (70kDa FITC-Dextran) labeling vessels depicted in green and grayscale. Soma of ensheathing pericytes are indicated with arrows. Baseline vessel diameter is indicated (dashed blue lines) to demonstrate ACT zone constriction following capillary regression.
(D) Graphs of percent change in the diameter of vessel segments throughout the microvascular zones (PA, ACT, Capillary, AV) of sham/repair and regression (regress.) events in animals that underwent anesthetized (blue) or awake (pink) imaging. Change from pre-injury is shown during the acute (3 or 7 days) and chronic (14 or 21 days) phase following capillary injury. Tukey's or Dunn's multiple comparison tests were performed depending on distribution of data. ACT zone: Acute: anesthetized sham/repair vs. regression ***p=0.0004; awake sham/repair vs. regression *p=0.014. Chronic: anesthetized sham/repair vs. regression *p=0.025; awake sham/repair vs. regression ***p=0.0006. Upstream capillary: Chronic: anesthetized regression vs. awake regression ***p=0.0002. Each datapoint is the diameter from a single vessel segment. Anesthetized: sham/repair = 10 experiments in 4 mice; regression = 9 experiments in 6 mice. Awake: sham/repair = 6 experiments in 3 mice; regression = 5 experiments in 4 mice.

Figure 4 – Capillary injury site does not influence arteriole-capillary transition zone constriction.

(A) Graphical depiction of Euclidean distance between arteriole-capillary transition (ACT) zone and capillary injury site. **(A')** Euclidean distance between ACT zone and injury site in sham/repair (black) and regression (purple) events. Unpaired t-tests revealed no significant difference. **(B)** Scatter plots of Euclidean distance of ACT zone to capillary injury site versus ACT zone diameter change from baseline during the acute (3 or 7 days) and chronic (14 or 21 days) phases. Spearman's rank correlation tests did not show a correlation between diameter change and proximity to the injury site. (**C)** Graphical depiction of vessel distance between arteriole-capillary transition (ACT) zone and capillary injury site. **(C')** Shortest vessel distance between ACT zone and injury site between sham/repair (black) and regression (purple) events. Unpaired t-tests revealed no significant difference. **(D)** Scatter plots of vessel distance versus ACT zone diameter change from baseline during the acute (3 or 7 days) and chronic (14 or 21 days) phases. Sham/repair = 16 experiments in 7 mice; regression = 14 experiments in 10 mice.

Figure 5 – Capillary regression uncouples mural cell-Ca^{2+} signaling and reduced vessel dynamics along the arteriole-capillary transition zone.

(A) Representative *in vivo* t-series image of arteriole-capillary transition (ACT) zones from a regression and repair event in an awake PdgfrβCre-GCaMP6f mouse. Pericytes are shown in green and i.v. dye (70kDa Texas Red-Dextran) labeling vessels depicted in red. In respective grayscale images, an example of vessel diameter (yellow crosslines) and GCaMP6 fluorescent intensity (yellow outline) analysis is shown.

(B) Scatter plots of change in mural cell-GCaMP6f signal (dF/F0) versus ACT zone diameter over at least 2 minutes (data point collected every 0.512s or 1.951Hz) pre-injury, acute (3 or 7 days post-injury) and chronic (14 or 21 days post-injury). Plots are shown following cross-correlation analysis (Supplementary Fig. 6B) with strongest correlation time shift shown. Regression correlation time: Pre t=2.048s, Acute t=1.536s, Chronic t=1.024s; Repair correlation time: Pre t=1.024s, Acute t=1.024s, Chronic t=1.536s. Spearman's rank correlations were performed, and respective r and p values are reported on graphs along with the coupling slope (S). **(C-E)** Graphs of **(C)** coupling slope, **(D)** diameter variance, and **(E)** mural cell-Ca^{2+} variance over the course of 21 days following injury in penetrating arterioles and ACT zones upstream of sham/repair (black) and regression (purple) events. Dunnett's multiple comparison test: Coupling slope: ACT zone - Regression event: 0 vs. 3 days: *p=0.0121, 0 vs. 7 days: *p=0.0105, 0 vs 14 days: *p=0.0229. Diameter variance: ACT zone - Regression event: 0 vs. 7 days: **p=0.0091, 0 vs. 21 days:

p=0.0091. Sham/repair n=5, regression n=5; 4 mice. **(F) Schematic demonstrating that capillary regression results in attenuated vasomotion (orange) and uncoupling of mural cell-Ca^{2+} signaling (black) in the upstream ACT zone.

Figure 6 – Capillary regression and chronic constriction of arteriole-capillary transition results in hypoperfusion of secondary off-shoot vessels.

(A) Graph of upstream arteriole-capillary transition (ACT) zone blood volume flux over the course of 21 days following sham/repair (black) and regression (purple) events. Dunnett's multiple comparison test: Regression event: 0 vs. 3 days: **p=0.0026. Sham/repair n=4, regression n=5; 4 mice.

(B, C) Graphs of **(B)** red blood cell (RBC) flux and **(C)** vessel diameter change over the course of 21 days following injury in secondary off-shoot capillaries following sham/repair (black) and regression (purple) events. Dunnett's multiple comparison test: RBC flux: Regression event: 0 vs. 3 day **p=0.0013, 0 vs. 21 days: ***p=0.0005.

(D) Scatter plot of ACT zone blood volume flux versus RBC flux in secondary off-shoots over 21 days post-injury in sham/repair (black) and regression (purple) events. Spearman's rank correlations were performed, respective r and p values are reported on graphs.

(E) Schematic demonstrating that capillary regression results in ACT zone constriction reducing blood flow into the microvascular network including uninjured, secondary off-shoot capillaries.

A

Capillary injury using two-photon irradiation

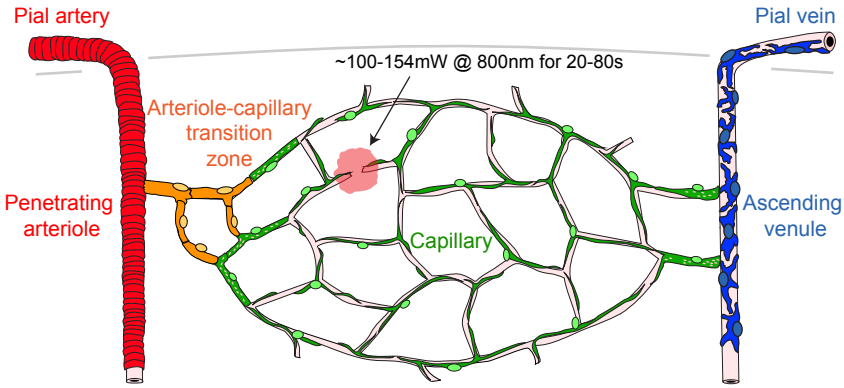

A'

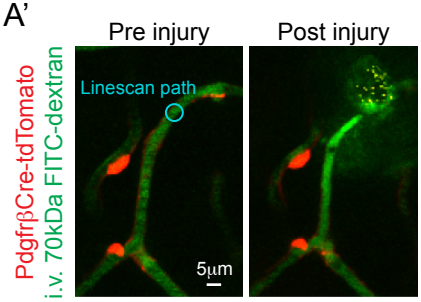

B

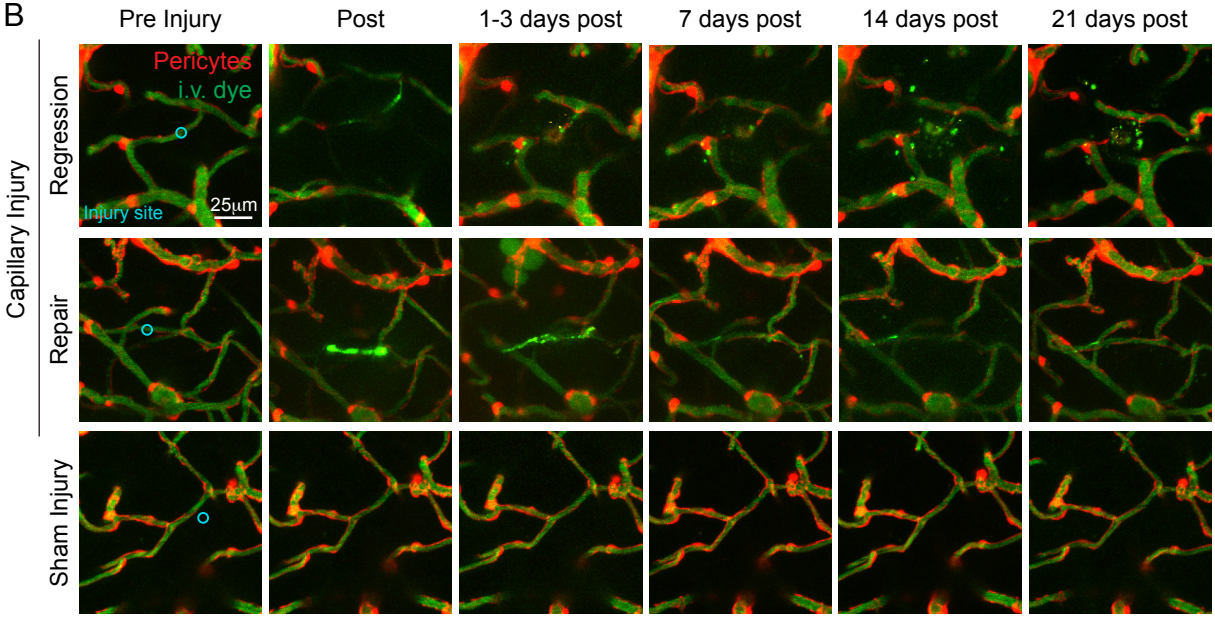

C

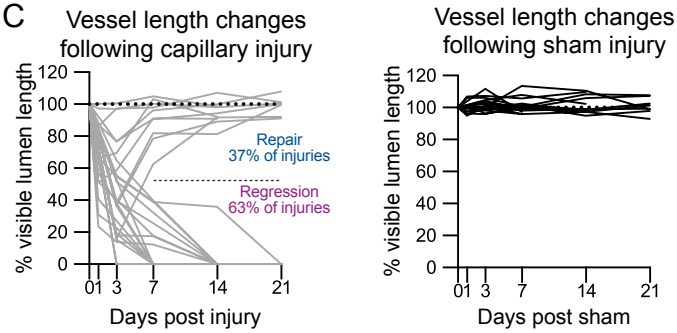

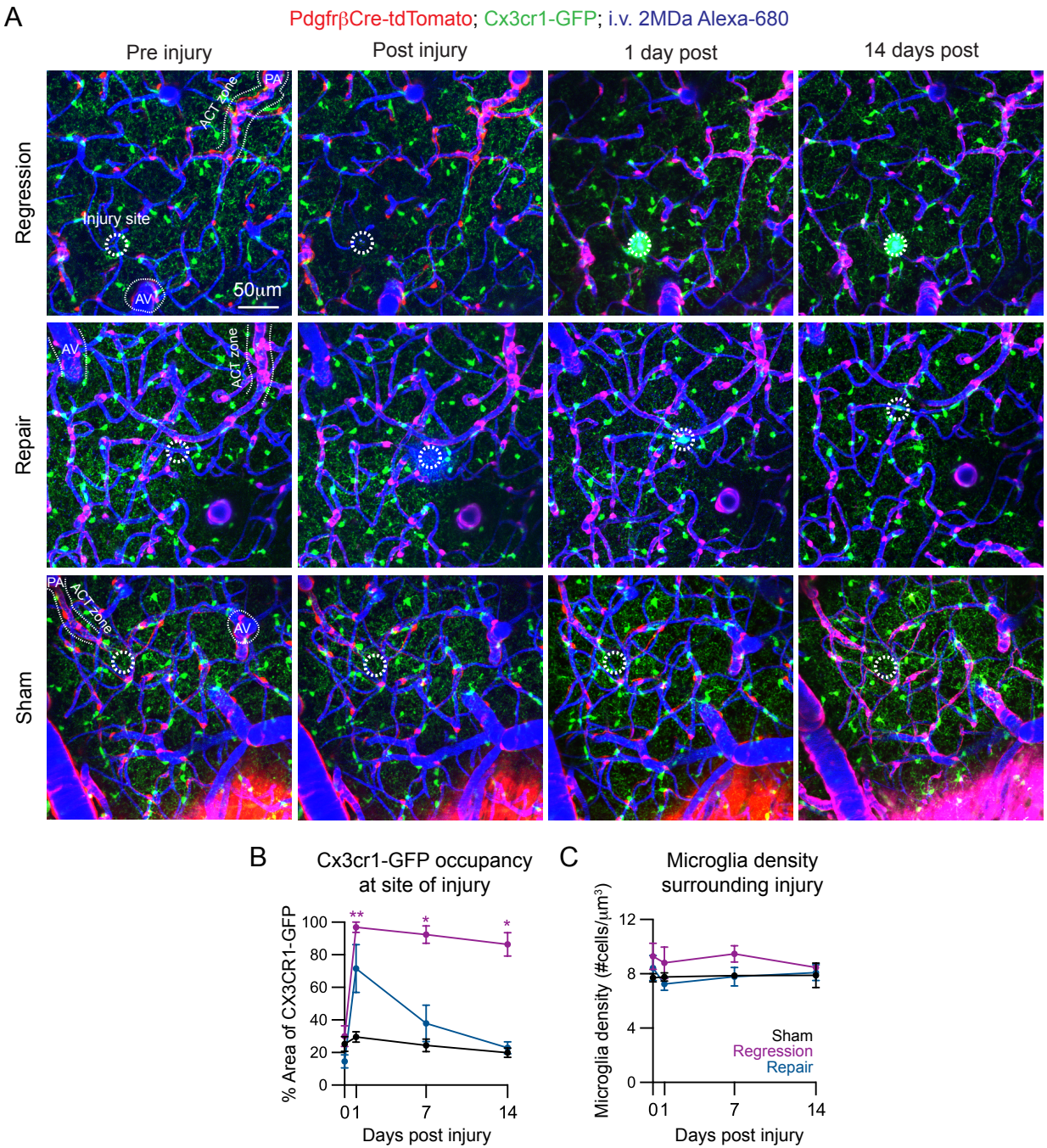
A
PdgfrβCre-tdTomato; Cx3cr1-GFP; i.v. 2MDa Alexa-680
Pre injury
Post injury
1 day post
14 days post
Regression
Repair
Sham
ACT zone
PA
AV
Injury site
50μm
B
Cx3cr1-GFP occupancy at site of injury
% Area of CX3CR1-GFP
Days post injury
C
Microglia density surrounding injury
Microglia density (#cells/μm³)
Sham
Regression
Repair
Days post injury

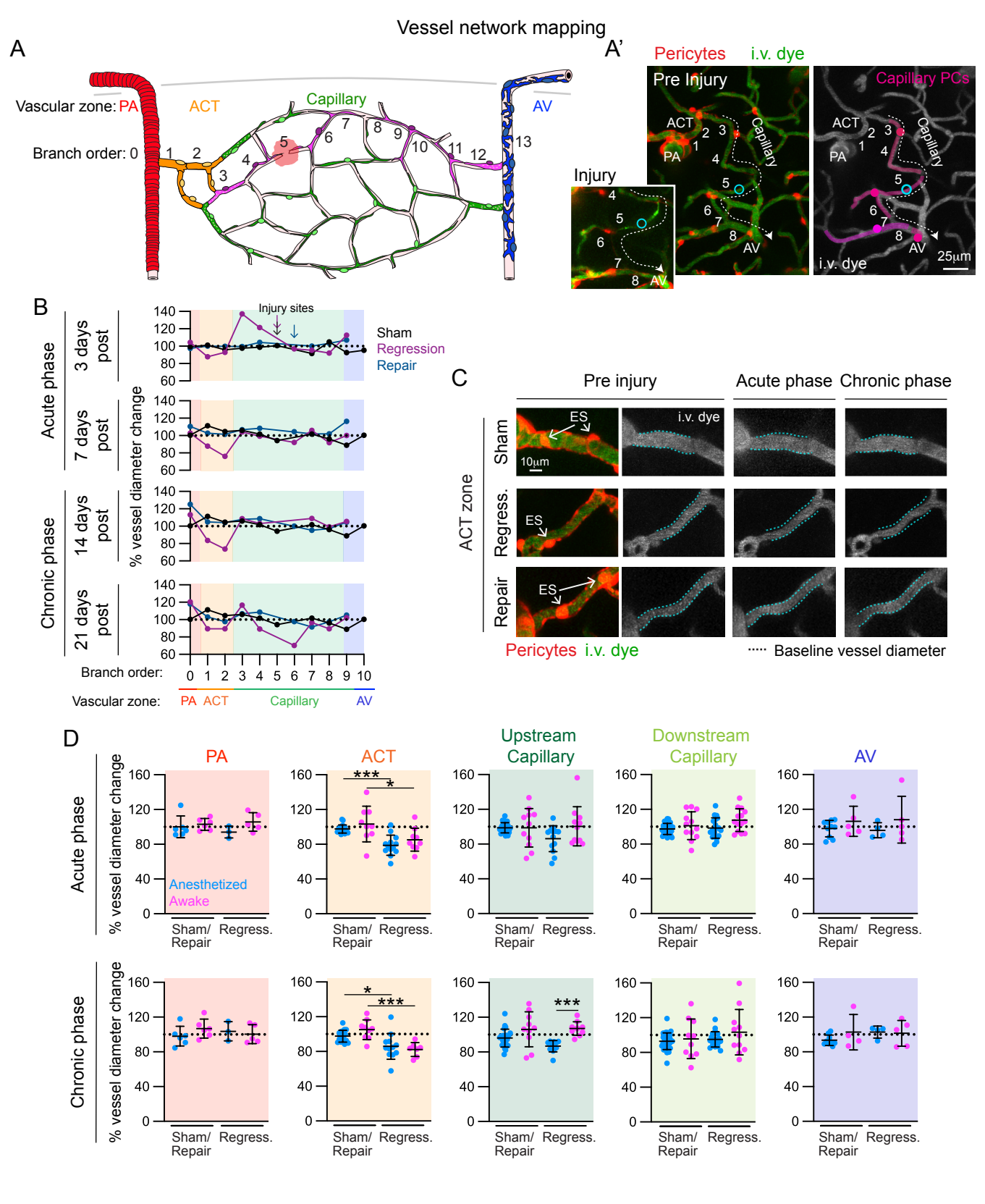
Vessel network mapping
A
Vascular zone: PA
ACT
Capillary
AV
Branch order: 0
1 2 3 4 5 6 7 8 9 10 11 12 13
A'
Pericytes
i.v. dye
Pre Injury
Injury
Capillary PCs
ACT
PA
Capillary
AV
i.v. dye
25µm
B
Acute phase
Chronic phase
3 days post
7 days post
14 days post
21 days post
% vessel diameter change
Injury sites
Sham
Regression
Repair
Branch order:
Vascular zone:
PA ACT Capillary AV
C
Pre injury
Acute phase
Chronic phase
ACT zone
Sham
Regress.
Repair
ES
i.v. dye
10µm
Pericytes i.v. dye
Baseline vessel diameter
D
PA
ACT
Upstream Capillary
Downstream Capillary
AV
Acute phase
Chronic phase
% vessel diameter change
Anesthetized
Awake
Sham/ Repair
Regress.

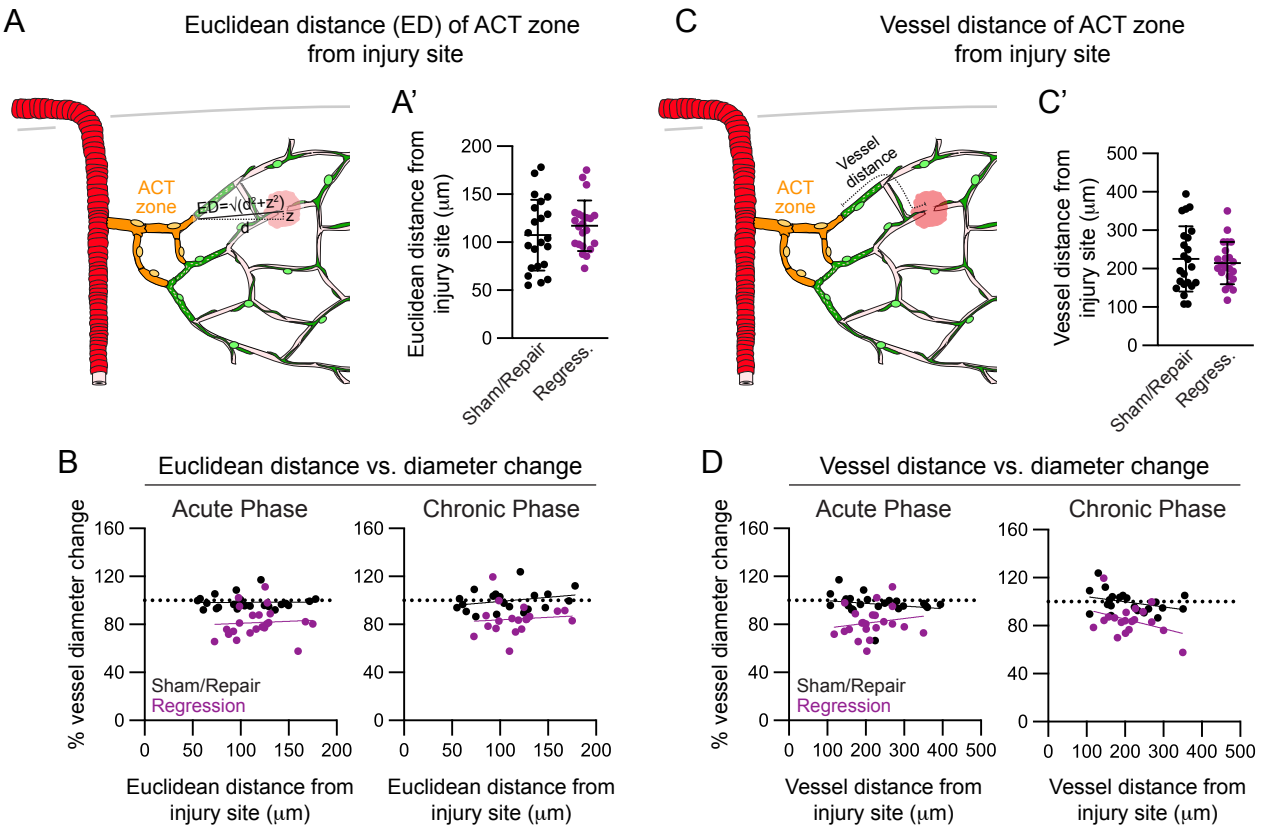
A
Euclidean distance (ED) of ACT zone from injury site
ACT zone
ED=√(d²+z²)
d
z
A'
Euclidean distance from injury site (μm)
200
150
100
50
0
Sham/Repair
Regress.
C
Vessel distance of ACT zone from injury site
ACT zone
Vessel distance
C'
Vessel distance from injury site (μm)
500
400
300
200
100
0
Sham/Repair
Regress.
B
Euclidean distance vs. diameter change
Acute Phase
Chronic Phase
% vessel diameter change
160
120
80
40
0
Sham/Repair
Regression
0
50
100
150
200
Euclidean distance from injury site (μm)
D
Vessel distance vs. diameter change
Acute Phase
Chronic Phase
% vessel diameter change
0
100
200
300
400
500
Vessel distance from injury site (μm)

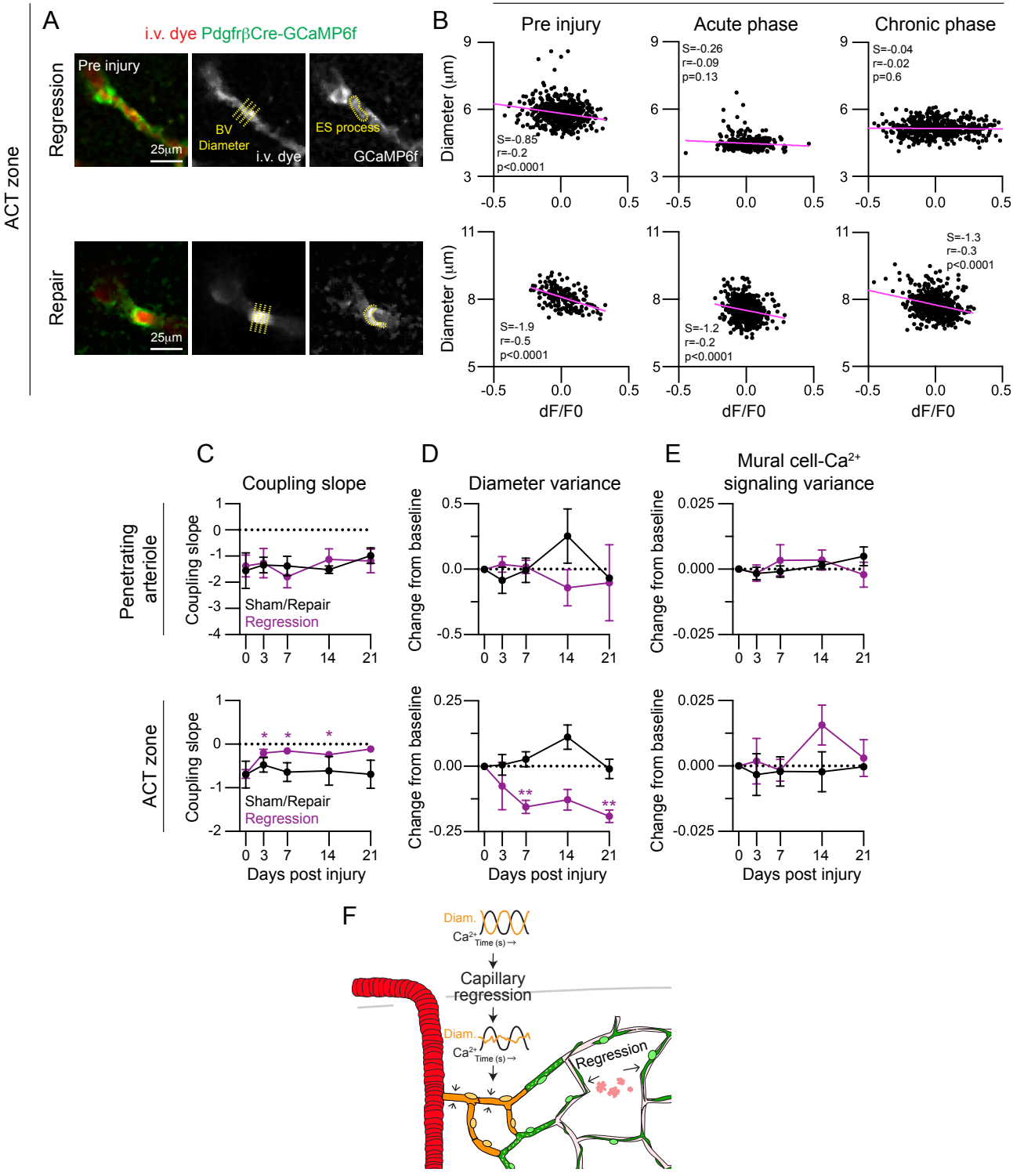
A
i.v. dye PdgfrβCre-GCaMP6f
ACT zone
Regression
Repair
Pre injury
25μm
BV
Diameter
i.v. dye
ES process
GCaMP6f
B
Mural cell-Ca2+ vs. diameter
Pre injury
Acute phase
Chronic phase
Diameter (μm)
S=-0.85
r=-0.2
p<0.0001
S=-0.26
r=-0.09
p=0.13
S=-0.04
r=-0.02
p=0.6
S=-1.9
r=-0.5
p<0.0001
S=-1.2
r=-0.2
p<0.0001
S=-1.3
r=-0.3
p<0.0001
dF/F0
C
Coupling slope
Penetrating arteriole
ACT zone
Sham/Repair
Regression
Days post injury
D
Diameter variance
Change from baseline
E
Mural cell-Ca2+ signaling variance
F
Diam.
Ca2+
Time (s)
Capillary regression
Regression

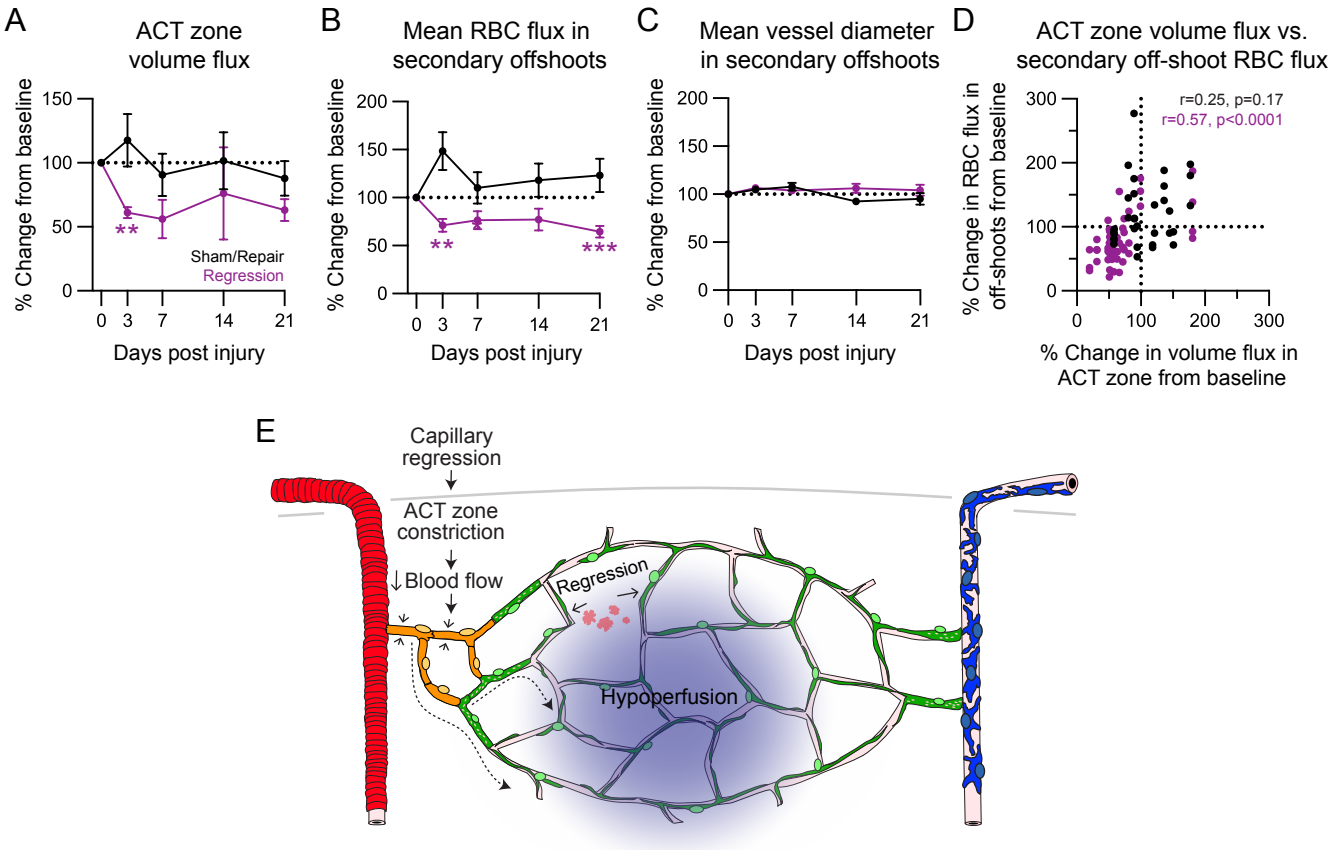
A
ACT zone volume flux
% Change from baseline
150
100
50
0
**
Sham/Repair
Regression
0 3 7 14 21
Days post injury
B
Mean RBC flux in secondary offshoots
% Change from baseline
200
150
100
50
0
**
***
0 3 7 14 21
Days post injury
C
Mean vessel diameter in secondary offshoots
% Change from baseline
200
150
100
50
0
0 3 7 14 21
Days post injury
D
ACT zone volume flux vs. secondary off-shoot RBC flux
% Change in RBC flux in off-shoots from baseline
300
200
100
0
r=0.25, p=0.17
r=0.57, p<0.0001
0 100 200 300
% Change in volume flux in ACT zone from baseline
E
Capillary regression
ACT zone constriction
↓Blood flow
Regression
Hypoperfusion